Title

Excitatory and suppressive receptive field subunits in awake monkey primary visual cortex (V1)

Journal

Proceedings of the National Academy of Sciences of the United States of America, 104

ISSN

0027-8424

Authors

Chen, Xiaodong
Han, Feng
Poo, Mu-ming
et al.

Publication Date

2007-11-01

Peer reviewed

Classification: Biological Sciences/Neuroscience

Excitatory and Suppressive Receptive Field Subunits in Awake Monkey V1

Xiaodong Chen[1], Feng Han[2], Mu-ming Poo[1,3] & Yang Dan[2,3]

1. Institute of Neuroscience, Shanghai Institutes for Biological Sciences, Chinese Academy of Sciences, 320 Yue-Yang Road, Shanghai, 200031, China
2. Group in Vision Science, University of California, Berkeley, CA 94720
3. Helen Wills Neuroscience Institute & Department of Molecular and Cell Biology, University of California, Berkeley, CA 94720

Correspondence:
Mu-ming Poo, Phone: 510-642-2514; Email: mpoo@berkeley.edu
Yang Dan, Phone: 510-643-2833; Email: ydan@berkeley.edu

Manuscript information: 23 pages, 7 figures
Word counts: 174 words in abstract; 34,198 characters in text

Abstract

An essential step in understanding visual processing is to characterize the neuronal receptive fields (RFs) at each stage of the visual pathway. However, RF characterization beyond V1 simple cells remains a major challenge. Recent application of spike-triggered covariance (STC) analysis has greatly facilitated characterization of complex cell RFs in anesthetized animals. Here we apply STC to RF characterization in awake monkey V1. We found up to 9 subunits for each cell, including one or two dominant excitatory subunits as described by the standard model, along with additional excitatory and suppressive subunits with weaker contributions. Compared to the dominant subunits, the non-dominant excitatory subunits prefer similar orientations and spatial frequencies but have larger spatial envelopes. They contribute to response invariance to small changes in stimulus orientation, position, and spatial frequency. In contrast, the suppressive subunits are tuned to orientations 45-90^{o} different from the excitatory subunits, which may underlie cross-orientation suppression. Together, the excitatory and suppressive subunits form a compact description of RFs in awake monkey V1, allowing prediction of the responses to arbitrary visual stimuli.

Introduction

The response properties of V1 neurons have been studied extensively over the past several decades. In the standard model, a simple cell RF consists of alternating ON and OFF subregions, which directly correspond to the orientation and spatial frequency tuning of the cell (1, 2). Complex cells exhibit orientation and spatial frequency tuning similar to simple cells, but they are insensitive to the contrast polarity and stimulus position within the RF. The energy model for complex cell RF consists of a pair of simple-cell-like subunits with the same orientation and spatial frequency tuning but different ON/OFF phases (3, 4). This model accounts for the phase invariance as well as stimulus selectivity of complex cells.

To validate such RF models and to predict the neuronal responses to arbitrary visual stimuli, it is necessary to measure the RF structure quantitatively. For simple cells, spike-triggered average (STA) has been used effectively to estimate their RFs from the responses to sparse noise (5) or white noise (6). For complex cells, however, since the outputs of different RF subunits are combined nonlinearly, these subunits cannot be estimated by STA. In previous studies, complex cell RFs have been studied by measuring the nonlinear interaction between paired stimuli (3, 7, 8). Another method used in recent studies is spike-triggered covariance (STC) analysis (9, 10). Instead of averaging all the stimuli preceding spikes (as in STA), in STC analysis one computes the covariance matrix of the spike-triggered stimulus ensemble and identifies the eigenvectors with eigenvalues significantly different from those of the entire stimulus ensemble. This method can reveal stimulus features that drive the neuron in a contrast-dependent but

polarity invariant manner, and it has proved highly effective in characterizing complex cell RF subunits in both cat (11, 12) and monkey (13) V1.

While the above studies have characterized the spatiotemporal structure of complex cell RFs in anesthetized animals, an ultimate challenge is to understand RF properties in the awake brain. Neuronal RFs in awake monkey V1 have been studied in phase-separated Fourier space (14). In the current study, we used STC to analyze the spatial structure of V1 RFs in awake monkeys. In addition to the dominant subunits that are consistent with the standard models for simple (1, 2) and complex (3, 4) cells, we found additional excitatory subunits that contribute to orientation, position, and spatial frequency invariance. For some cells, we also found suppressive subunits (13). These subunits are tuned to orientations up to 90^o different from the excitatory subunits, which may contribute to cross-orientation suppression (15). Including the non-dominant excitatory and suppressive subunits in the model significantly improved the prediction of neuronal responses to arbitrary white noise stimuli.

Results

We made single-unit recordings from 227 V1 neurons in three macaque monkeys performing a fixation task. Visual stimuli were binary white noise (10×10 – 12×12 pixels, 25 frames/s) presented in an area slightly larger than the RF of each cell. During each stimulus epoch (7500 frames, 5 min), the eye position was monitored continuously. Recordings during periods when the eye position was outside of a fixation window were excluded from analyses (Fig. 1A).

The stimulus preceding each spike was collected to form the spike-triggered ensemble (Fig. 1B), and the covariance matrix of this ensemble was computed. Significant eigenvalues were identified as those that were significantly different from (1) the control eigenvalues calculated based on randomized spike trains (Fig. 2A) and (2) their neighboring eigenvalues (Fig. 2B) (16) (Materials and Methods). For 145 of the 227 cells studied, we found at least one significant eigenvalue. The eigenvectors with significantly higher eigenvalues represent stimulus features that excite the cell (11, 16), whereas those with significantly lower eigenvalues reflect suppressive features that reduce neuronal firing (13).

Grouping of significant eigenvectors

The significant eigenvectors of each cell could be divided into three groups, based on their spatial structure and eigenvalues. The first group consisted of one or two eigenvectors, whose eigenvalues stood out most prominently above the rest. These excitatory eigenvectors, referred to as “dominant eigenvectors”, were almost always

Gabor-like. Most of the complex cell-like neurons, whose responses to drifting gratings were only weakly modulated at the stimulus temporal frequency (17), contained a pair of dominant eigenvectors (e.g., both cells in Fig. 2). These eigenvectors were similar to each other in size, orientation, and spatial frequency, but different in phase (Fig. 2C), consistent with the pair of subunits in the energy model (3, 4). On the other hand, cells with strong temporal modulations (simple cell-like) are likely to have a single dominant eigenvector (i.e., the largest jump is between the first and second eigenvalues). This eigenvector typically resembled STA (data not shown), which represents the linear RF of the simple cell. Note that we did not strictly distinguish between simple and complex cells because recent studies suggested that V1 neurons fall on a simple/complex continuum rather than two distinct classes (18, 19).

Many simple- or complex-like neurons also exhibited additional excitatory eigenvectors, whose eigenvalues showed smaller but significant upward jumps (Fig. 2A, 2B). This second group of eigenvectors, referred to as “non-dominant” excitatory eigenvectors, were oriented similarly to the dominant eigenvectors but showed more complex spatial structures and larger sizes (Fig. 2C, 3A). For 38 cells, we also found a third group of eigenvectors with significantly lower eigenvalues. Most of these suppressive eigenvectors (Fig. 2, second cell; Fig. 3A, third and fourth cells) are oriented differently from the excitatory eigenvectors. It is important to note that, although the significant eigenvectors provide a functional description of the RF that is indicative of the response properties of the presynaptic neurons, each significant eigenvector does not necessarily represent the RF of an individual presynaptic cell (i.e., an “anatomical subunit”). Instead, it is likely to represent a linear combination of multiple anatomical

subunits (11, 13). However, as a convenient functional description, we refer to these significant eigenvectors as the excitatory or suppressive RF subunits.

Relationship between subunit groups

To understand the relationship between the three groups of subunits, we first compared their locations and sizes by computing the pooled spatial envelope of each group (square root of the weighted sum of squares of all the subunits in each group, see Materials and Methods) (13). Compared to the dominant group, the non-dominant excitatory subunits showed a larger spatial envelope (Fig. 4A, 4C), similar to the finding in anesthetized monkey V1 (13). This could be explained if the non-dominant eigenvectors represent combinations of multiple anatomical subunits that are spatially displaced from each other. The suppressive subunits, on the other hand, largely overlapped with the dominant subunits in space. Quantitative comparison of the subunit sizes is summarized in Fig. 5A and 5B, based on the width-at-half-height of each pooled envelope along the preferred orientation (length) and the perpendicular axis (width).

We also compared the spatial frequency and orientation tuning of the three groups based on the pooled spatial spectrum of each group (Fig. 4B). The spectrum of the non-dominant excitatory group largely overlapped with that of the dominant group (Fig. 4C), indicating similar orientation and frequency tuning. In contrast, the spectrum of the suppressive subunits showed little overlap with the excitatory groups. The separation between the excitatory and suppressive subunits in spatial spectrum was more pronounced along the angular than the radial axis, indicating major differences in orientation as opposed to frequency tuning. For the population of cells, the preferred

spatial frequency and orientation of the non-dominant excitatory subunits were closely correlated with those of the dominant subunits (Fig. 5C, 5D, upper panel), but the suppressive subunits showed larger deviations in frequency tuning and up to 90^{o} difference in preferred orientation (lower panel).

Response invariance

The angular separation between the excitatory and suppressive subunits in the spectral domain suggests that the suppressive subunits contribute to cross-orientation suppression (15), which should enhance the selectivity of V1 neurons. What is the function of the non-dominant excitatory subunits? Since each excitatory eigenvector is likely to represent a combination of multiple anatomical subunits (11, 13), and conversely an anatomical subunit may be approximated as a combination of eigenvectors, we examined various linear combinations of the excitatory eigenvectors. The neuronal responses to combinations of eigenvectors can be characterized by joint contrast-response functions (11, 13).

Figure 6A shows the joint contrast-response functions for four pair-wise combinations of the excitatory subunits of a neuron. The contrast of a given subunit in each stimulus is defined as the dot product of the eigenvector and the stimulus, and the neuronal firing rate is plotted against the contrasts of each pair of subunits. Consistent with previous findings in cat V1 (11), each combination of the dominant pair of subunits is also Gabor-like (Fig. 6A, top left), with the spatial phase shifting with the relative weights of the two subunits (angular coordinate of the 2-D function). The circularly symmetric joint contrast-response function is thus consistent with the known phase

invariance of complex cells (1, 3, 4). Interestingly, combinations between a dominant and a non-dominant excitatory subunit revealed other forms of invariance. For this cell, although the third (non-dominant) eigenvector contained fractured ON and OFF subregions, its combinations with the first (dominant) eigenvector resulted in Gabor-like patterns at different orientations (upper right plot, compare patterns in the 3 boxes). Furthermore, combinations between the second and third eigenvectors resulted in Gabor patterns at different positions (lower left plot), and those between the second and fifth exhibited different frequencies (lower right plot). Since the non-dominant subunits make weaker contributions to the response than the dominant ones, the joint contrast-response functions did not exhibit perfect circular symmetry. Nevertheless, the existence of these weaker excitatory subunits enhanced the response invariance with respect to small changes in stimulus orientation, position, and frequency (20). A plausible anatomical basis for such invariance is that the neuron receives inputs from a set of presynaptic neurons with slightly different preferred orientations, RF positions, and spatial frequencies.

The above three types of invariance were also observed in other cells, with orientation invariance the most common. We thus further quantified the effect of non-dominant excitatory subunits on orientation tuning. The tuning of each subunit was computed as its responses to sinusoidal gratings at a range of orientations at the optimal frequency. Since previous studies have shown that the excitatory subunits contribute additively to the responses (11, 13), the tuning of the cell was predicted as the weighted sum of the tuning of all excitatory subunits, with the weight of each subunit proportional to its contrast-response gain (Materials and Methods). As shown in Fig. 6B, including the

non-dominant excitatory subunits in the prediction indeed broadened the tuning for this example cell. For the population of cells with well-tuned excitatory subunits, including the non-dominant subunits significantly increased the width of tuning (Fig. 6C, $p < 0.01$, Wilcoxon signed rank test). Notably, the effects of the non-dominant excitatory subunits and the suppressive subunits on orientation tuning do not simply cancel each other. While the non-dominant excitatory subunits render the neuron less sensitive to small variations around the optimal orientation, the suppressive subunits reduce the responses near the orthogonal orientation without necessarily narrowing the tuning curve (Fig. 6B, inset).

Predictions of responses to white noise

Finally, to assess the RF model based on the significant eigenvectors, we predicted the response of each cell to a short white-noise test sequence (30 s, repeated 4-70 times) using (I) dominant subunits alone, (II) all excitatory subunits, and (III) all excitatory and suppressive subunits. The responses of the excitatory subunits and those of the suppressive subunits were first summed separately using weights proportional to their contrast-response gains. The excitatory and suppressive components were then combined with a nonlinear function that allows both subtractive and divisive interactions (13) (Materials and Methods). Figure 7A shows the measured response of an example cell (gray shading) and the predictions based on the dominant subunits alone (black line) and based on all excitatory and suppressive subunits (red line). Although the model based on the dominant subunits alone predicted the main temporal variations of the response, including the non-dominant excitatory and suppressive subunits improved the prediction by alleviating both under- and over-estimation of the peak amplitudes (Fig. 7A, arrow heads).

We measured the quality of prediction by each model using correlation coefficient between the predicted and measured responses. Compared to the model based on the dominant subunits alone, including the non-dominant excitatory subunits significantly improved the prediction for the population of cells (Fig. 7B, $p < 10^{-5}$, Wilcoxon signed rank test, n = 83). Including the suppressive subunits led to a small further improvement (Fig. 7C), although the effect was not significant. Even with the full model, however, the correlation coefficient between the predicted and measured responses was lower than that between measured responses averaged from different repeats (Fig. 7D), indicating that the prediction error could not be entirely accounted for by noise in the measured responses. The incompleteness of the model may be due to additional subunits not identified by STC or to inaccuracy in the estimated RF subunits, both of which depend on the amount of data (21, 22) that is limited in recordings from awake monkeys. More importantly, the responses are likely to exhibit other forms of nonlinearity such as adaptation (23), which are not captured by the RF model used in this study.

Discussion

The current study, together with several other STC analyses (11-13, 16), suggests the following model for V1 classical RF. The dominant RF component is a Gabor-like subunit for simple cells and a pair of subunits for complex cells, consistent with the standard model (1-4). In both anesthetized and awake monkeys, however, STC analysis allowed identification of two additional groups of subunits: the non-dominant excitatory and suppressive subunits, whose contributions to V1 responses are weaker than the dominant subunits. The non-dominant excitatory subunits are more dispersed spatially but largely overlap with the dominant subunits in the frequency spectrum (Figs. 4, 5), and

they contribute to response invariance to small changes in stimulus orientation, position, and frequency (Fig. 6). In contrast, the suppressive subunits overlap with the dominant subunits spatially but are complementary in the frequency spectrum. They are likely to mediate suppression of the responses to "antagonistic" visual features such as those at the orthogonal orientation (Figs. 4, 5). Invariance and selectivity of neuronal responses are both important for visual processing. As shown in Fig. 7, incorporating the non-dominant subunits in the model improves the prediction of responses to arbitrary white noise stimuli.

In previous studies in anesthetized cat V1 (11, 12, 16), we found that most complex cell RFs consist of two Gabor-like subunits, and non-dominant subunits were rarely observed. In this study, it is possible that small eye movements within the fixation window produced artifactual significant eigenvectors and contributed to the non-dominant subunits. Although we cannot exclude this possibility completely, the finding that the non-dominant subunits significantly improved the response prediction (Fig. 7) indicates that they are integral components of the functional description of V1 responses. The difference in the number of significant eigenvectors found in the current and previous studies may be partly due to differences in the number of spikes used in the analysis, the signal/noise ratio of the responses, or the number or strength of the non-dominant subunits. Regardless of the underlying reason, the fact that non-dominant subunits are readily observed in V1 of both anesthetized (13) and awake monkeys suggests that there are significant inter-species differences in the number of RF subunits identifiable by the STC analysis.

The effect of the non-dominant subunits in improving response prediction found in this study (Fig. 7) is relatively small compared to that found in anesthetized monkey V1 (13). This discrepancy may be partly due to the difference in the stimuli used for testing the models. While we used arbitrary white noise stimuli, the test stimuli used previously were matched to the non-dominant subunits in spatiotemporal patterns and are thus likely to emphasize their contributions to the responses. It is also possible that, compared to the 2-D white noise stimuli used in this study, the relative contribution of the non-dominant subunits is stronger in response to bar stimuli at the preferred orientation (13). Nevertheless, it is interesting to note that both null-direction and cross-orientation suppression can be modeled by suppressive RF subunits, even though they are likely to be mediated by distinct neural circuits.

Most of the previous quantitative studies of neuronal RFs were performed under anesthesia, which may significantly affect the response properties of sensory neurons. Our study shows that STC analysis is highly effective for mapping RF subunit structure in awake monkey V1. While this study is performed with white noise stimuli, a similar technique can be used to analyze cortical responses to naturalistic stimuli (12, 14, 16, 24). The findings reported here not only provide a compact RF model for understanding V1 responses to arbitrary stimuli (Fig. 7), but also set the stage for studying nonlinear visual processing in higher-level cortical areas.

Materials/Methods

Recording

Single-unit recordings were made in V1 of 3 adult monkeys (*Macaca mulatta,* 2 male, 1 female) using glass-coated tungsten electrodes (25). Unit isolation was based on cluster analysis of waveforms and the presence of a refractory period in autocorrelograms. Each recording epoch was 5 min. All single units lasting for ≥3 epochs were included (maximum 25 epochs, n = 227). The RFs of these cells were 2-9^{o} from the fixation point. During each epoch, the monkey performed a continuous fixation task for juice reward. Eye position was monitored with a remote, infrared eye tracker (EYELINK II, resolution 0.01º, sampling rate 500 Hz). An elliptical window was set for eye position; vertical and horizontal axes were selected so that the kurtosis of data points in the window was 3 (mean vertical axis, 1.2^{o}; horizontal axis, 0.5^{o}). Data recorded while the eye position was outside of the window were discarded (Fig. 1). In practice, however, our results were quite insensitive to the window size or shape; results were similar even when it was set to infinity. Surgery was conducted under aseptic conditions under deep pentobarbital anesthesia. All procedures were in accordance with the NIH guidelines.

Visual stimulation

Stimuli were generated with a PC, presented with a Sony Multiscan G520 monitor (30×40 cm, refresh rate 100 Hz, maximum luminance 80cdm^{-2}). Binary white noise (10×10 – 12×12 pixels, 0.8×0.8^{o} – 4.2×4.2^{o}, 100% contrast) was presented at an effective frame rate of 25 Hz (updated every 4 frames). Each epoch consisted of 7500 frames; stimuli in different epochs were different. To test prediction of the model based on

significant eigenvectors, a white noise sequence (750 frames, 30s) was repeated 4-70 times for each cell.

Spike-triggered covariance analysis

Details of the STC analysis have been described previously (11, 13, 16). Briefly, the STC matrix [$C_{m,n}$] was computed as

$$C_{m,n} = \frac{1}{N}\sum_{i=1}^{N} S_m(i)S_n(i)$$

$S_m(i)$ and $S_n(i)$ are luminance of the mth and nth pixels in the stimulus preceding the ith spike, N is the total number of spikes. Eigenvalues and eigenvectors of this matrix were computed. To identify significant eigenvectors, we first determined which eigenvalues are significantly different from the control (Fig. 2A), defined as the eigenvalues of spike-triggered ensembles based on random spike trains (with the same spike number as the recorded response but random spike time; the results are very similar if the controls are generated by shifting the recorded spike train randomly in time). The confidence intervals for the control were computed using 500 random spike trains (mean ± 4.4 SD, corresponding to $p<10^{-4}$ for Gaussian distribution; we found that the distribution of control eigenvalues was close to Gaussian). We then identified "outstanding" eigenvalues by calculating the difference between neighboring eigenvalues (Fig. 2B). The confidence interval was set at mean + 4.4 SD of the differences, after excluding the first and last five eigenvalues (which are likely to be significant eigenvalues with large differences from their neighbors). If a point is found beyond the confidence interval, all the eigenvalues preceding (for excitatory eigenvectors) or following (for suppressive eigenvectors) this

point are considered significant by this criterion (Fig. 2B). Eigenvalues that satisfy both criteria (Fig. 2A, 2B) are considered significant. Note that with Gaussian noise as stimuli, only the first criterion (Fig. 2A) is necessary. With binary stimuli, however, incorporating the second criterion (Fig. 2B) helps to reduce artifacts in identifying the suppressive subunits (see below). The 4.4 SD used for both criteria is of course somewhat arbitrary. Although we did not select cells based on spike number (all cells with ≥ 3 epochs were included), we found that the number of spikes significantly affected the probability of finding significant eigenvectors. Among the 18 cells with <3,000 spikes, only 2 (11%) had significant eigenvectors, but for the 186 cells with > 5,000 spikes, 128 (69%) had significant eigenvectors.

In most analyses (Figs. 2-6) we focused on the spatial RF structure by performing STC at the optimal frame (1 or 2 frames before each spike) to improve signal-to-noise ratio of the estimate. For predicting the responses to white noise stimuli (Fig. 7), both frames were included to estimate the spatiotemporal RF subunits. Although in principle including both frames should improve the prediction, in practice this improvement was very small, probably because including the second frame also reduced the accuracy of the estimated eigenvectors.

Note that to compute the standard covariance matrix, the average of the spike-triggered ensemble (STA) should be subtracted from the stimuli. In some implementations of STC, STA is weighted before subtracted to ensure that the eigenvectors are orthogonal to STA (13). We believe that the treatment of STA is largely a matter of individual preference, as long as the specific choice is taken into consideration when interpreting the result. As in our previous implementations (11, 16),

STA was not subtracted in this study. As a result, the first eigenvector (with largest eigenvalue) of simple-cell-like neurons is often similar to STA.

As pointed out in previous studies (13, 22), the use of binary white noise may result in artifacts in the identification of suppressive eigenvectors, due to tapering of the stimulus distribution (reduction of variance) as one moves away from the origin along particular directions. The resulting spurious suppressive eigenvectors are related to the excitatory eigenvectors that lie close to these directions rather than the suppressive features of the neuron. To reduce such artifacts, we used the method developed in a previous study (13). Briefly, we computed the pooled response of the excitatory eigenvectors to each stimulus, divided these stimuli into 10 equal-sized subsets according to the pooled responses, and whitened each subset by multiplying it by $E_e E_e^T + E_o E_n D_n^{-1/2} E_n^T E_o^T$. The matrix E_e contains the excitatory eigenvectors, E_o contains all other eigenvectors, and E_n and D_n are eigenvectors and eigenvalues of the covariance matrix of the *n*th subset. The whitened stimuli were then used to estimate the suppressive eigenvectors (13). The combination of this whitening step and the use of the second criterion (Fig. 2B) effectively eliminated the spurious suppressive eigenvectors.

Relative weights of subunits

The contribution of each significant eigenvector (V) to neuronal response depends on the gain of the contrast-response function. The gain was estimated by fitting the left and right sides of the function separately by $r = a(S \bullet V)^2 + b$, where r is the firing rate, S is the stimulus, a and b are free parameters (11, 16). The relative weight of each eigenvector is defined as $\sqrt{|a|}$, used to compute the pooled spatial envelope and Fourier

spectrum (Fig. 4) and the pooled responses for predicting orientation tuning (Fig. 6) and white noise responses (Fig. 7).

Response prediction

To predict the responses to arbitrary stimuli, we fitted the following function to recorded responses:

$$r = \alpha + (\beta E - \delta S)/(\gamma E + \varepsilon S + 1)$$

E and S are pooled responses of the excitatory and suppressive eigenvectors, respectively, and α, β, δ, γ, and ε are free parameters. This is similar to the model in a previous study (13), allowing both subtractive and divisive contributions of the suppressive eigenvectors. Values for the free parameters were fit to minimize the mean-squared error for the "training data", which are the responses used to compute the eigenvectors.

Acknowledgments

We thank Dr. Yu-Xi Fu for technical support. This work was supported by Outstanding Overseas Chinese Scholars Fund (2005-1-6), project KSCX2-YW-R-29 of Chinese Academy of Sciences, and a NEI grant.

References

1. Hubel, D. H. & Wiesel, T. N. (1962) *J Physiol (Lond)* **160,** 106-54.
2. Movshon, J. A., Thompson, I. D. & Tolhurst, D. J. (1978) *J Physiol* **283,** 53-77.
3. Movshon, J. A., Thompson, I. D. & Tolhurst, D. J. (1978) *J Physiol (Lond)* **283,** 79-99.
4. Adelson, E. H. & Bergen, J. R. (1985) *J Opt Soc Am A* **2,** 284-99.
5. Jones, J. P. & Palmer, L. A. (1987) *J Neurophysiol* **58,** 1187-1211.
6. Reid, R. C., Victor, J. D. & Shapley, R. M. (1997) *Vis Neurosci* **14,** 1015-1027.
7. Emerson, R. C., Citron, M. C., Vaughn, W. J. & Klein, S. A. (1987) *J Neurophysiol* **58,** 33-65.
8. Livingstone, M. S. & Conway, B. R. (2003) *J Neurophysiol* **89,** 2743-59.
9. De Ruyter Van Steveninck, R. & Bialek, W. (1988) *Proceedings of the Royal Society of London Series B Biological Sciences* **234,** 379-414.
10. Brenner, N., Bialek, W. & de Ruyter van Steveninck, R. (2000) *Neuron* **26,** 695-702.
11. Touryan, J., Lau, B. & Dan, Y. (2002) *J Neurosci* **22,** 10811-8.
12. Felsen, G., Touryan, J., Han, F. & Dan, Y. (2005) *PLoS Biol* **3,** e342.
13. Rust, N. C., Schwartz, O., Movshon, J. A. & Simoncelli, E. P. (2005) *Neuron* **46,** 945-56.
14. David, S. V., Vinje, W. E. & Gallant, J. L. (2004) *J Neurosci* **24,** 6991-7006.
15. Bonds, A. B. (1989) *Vis Neurosci* **2,** 41-55.
16. Touryan, J., Felsen, G. & Dan, Y. (2005) *Neuron* **45,** 781-91.

17. Skottun, B. C., De Valois, R. L., Grosof, D. H., Movshon, J. A., Albrecht, D. G. & Bonds, A. B. (1991) *Vision Res* **31,** 1079-86.

18. Chance, F. S., Nelson, S. B. & Abbott, L. F. (1999) *Nat Neurosci* **2,** 277-82.

19. Mechler, F. & Ringach, D. L. (2002) *Vision Res* **42,** 1017-33.

20. Berkes, P. & Wiskott, L. (2006) *Neural Comput* **18,** 1868-95.

21. Aguera y Arcas, B. & Fairhall, A. L. (2003) *Neural Comput* **15,** 1789-807.

22. Paninski, L. (2003) *Network* **14,** 437-64.

23. Maffei, L., Fiorentini, A. & Bisti, S. (1973) *Science* **182,** 1036-8.

24. Sharpee, T. O., Sugihara, H., Kurgansky, A. V., Rebrik, S. P., Stryker, M. P. & Miller, K. D. (2006) *Nature* **439,** 936-42.

25. Li, C. Y., Xu, X. Z. & Tigwell, D. (1995) *J Neurosci Methods* **57,** 217-20.

Figure Legends

Figure 1. Illustration of experimental and analysis procedures. (**A**) Example eye position traces recorded by the eye tracker. Scales: 1s, 1^{o}. Shading: periods with eye position outside of fixation window. Corresponding segments of the spike train (bottom) were excluded from analysis. Gray: excluded spikes. (**B**) White noise stimuli. Gray box: stimulus preceding each spike.

Figure 2. Identification of significant eigenvectors, illustrated with two V1 cells (left and right columns). (**A**) Eigenvalues of STC matrix. Dashed lines: control confidence intervals ($p<10^{-4}$). (**B**) Difference between neighboring eigenvalues. Dashed line: confidence interval for the difference ($p<10^{-4}$). Large circles: significant eigenvalues satisfying criteria in both (A) and (B). (**C**) Significant eigenvectors. Contrast of each eigenvector is scaled by its relative weight (see Materials and Methods). Excitatory and suppressive eigenvectors were scaled separately. Scale: 0.5°.

Figure 3. Number of significant eigenvectors per cell. (**A**) Significant eigenvectors for 4 example cells. E, excitatory, S, suppressive. Scale: 0.5°. (**B**) Distribution of the number of significant eigenvectors per cell.

Figure 4. Spatial and spectral relationships among subunit groups. (**A**) Top panel: Dominant and non-dominant excitatory (E_d and E_{nd}) and suppressive (S) subunits of a cell. Scale: 0.5^{o}. Bottom panel: pooled spatial envelope of each group of subunits. Red, E; green, S. In E&S (all groups superimposed), yellow indicates overlap between E and S. (**B**) Top panel: Spatial frequency spectrum of each subunit in (A). Bottom panel:

Pooled frequency spectrum of each group. (**C**) Pooled spatial envelopes (upper row) and frequency spectra (lower row) of the three subunit groups for five cells.

Figure 5. Quantitative comparison between non-dominant and dominant subunits. (**A**, **B**), Length and width of pooled spatial envelope, measured by width at half height. Each point represents one cell (n=79). (**C**) Optimal spatial frequency (peak of frequency spectrum) for the same cells in (A) and (B). (**D**) Difference in preferred orientation. White bars, cells with clear tuning (circular variance of tuning for each group of subunits <0.7); gray bars, poorly tuned cells (circular variance >0.7). Circular variance is defined as $1-\left|\sum_k R_k e^{i2\theta_k}\right| / \sum_k R_k$ (R_k: response at orientation θ_k, $0<\theta_k<180^o$).

Figure 6. Phase, orientation, position, and frequency invariance. (**A**) Joint contrast-response functions of a complex cell (second cell in Fig. 3A) for different pair-wise combinations of its 6 excitatory subunits. Firing rate is luminance coded. Black lines: contours of constant firing rate (at 0.5× and 1× mean of each function); circular contour indicates perfect invariance. Small outer plots: stimulus patterns corresponding to selected points (arrows) in the function. (**B**) Orientation tuning of the cell predicted by the dominant subunits alone (dashed) and by all excitatory subunits (solid). Arrows indicate width at half height. Inset, predicted tuning of another cell, based on only the excitatory subunits (dashed) and on both excitatory and suppressive subunits. (**C**) Predicted tuning width based on all excitatory subunits vs. that based on dominant subunits alone. Each point represents one cell; only cells with clear tuning (circular variance <0.6) were included (n=56).

Figure 7. Prediction of responses to white noise stimuli. (**A**) Comparison of predicted and measured firing rates of a cell. Gray shading: measured response averaged from 24 repeats of the test stimulus. Black line: Prediction based on dominant subunits. Red line: Prediction based on all subunits (6 excitatory, 1 suppressive). Red arrow heads, peaks better predicted by the model with all subunits. (**B**) Improvement of prediction by non-dominant excitatory subunits. Correlation coefficient (CC) between measured and predicted responses based on all excitatory subunits vs. CC with only dominant subunits. Each symbol represents one cell. (**C**) Improvement of prediction by suppressive subunits. CC based on both excitatory and suppressive subunits vs. CC with only excitatory subunits. (**D**) CC between measured responses (averaged from two non-overlapping sets of repeats) vs. CC between predicted (based on all subunits) and measured responses (n=123).

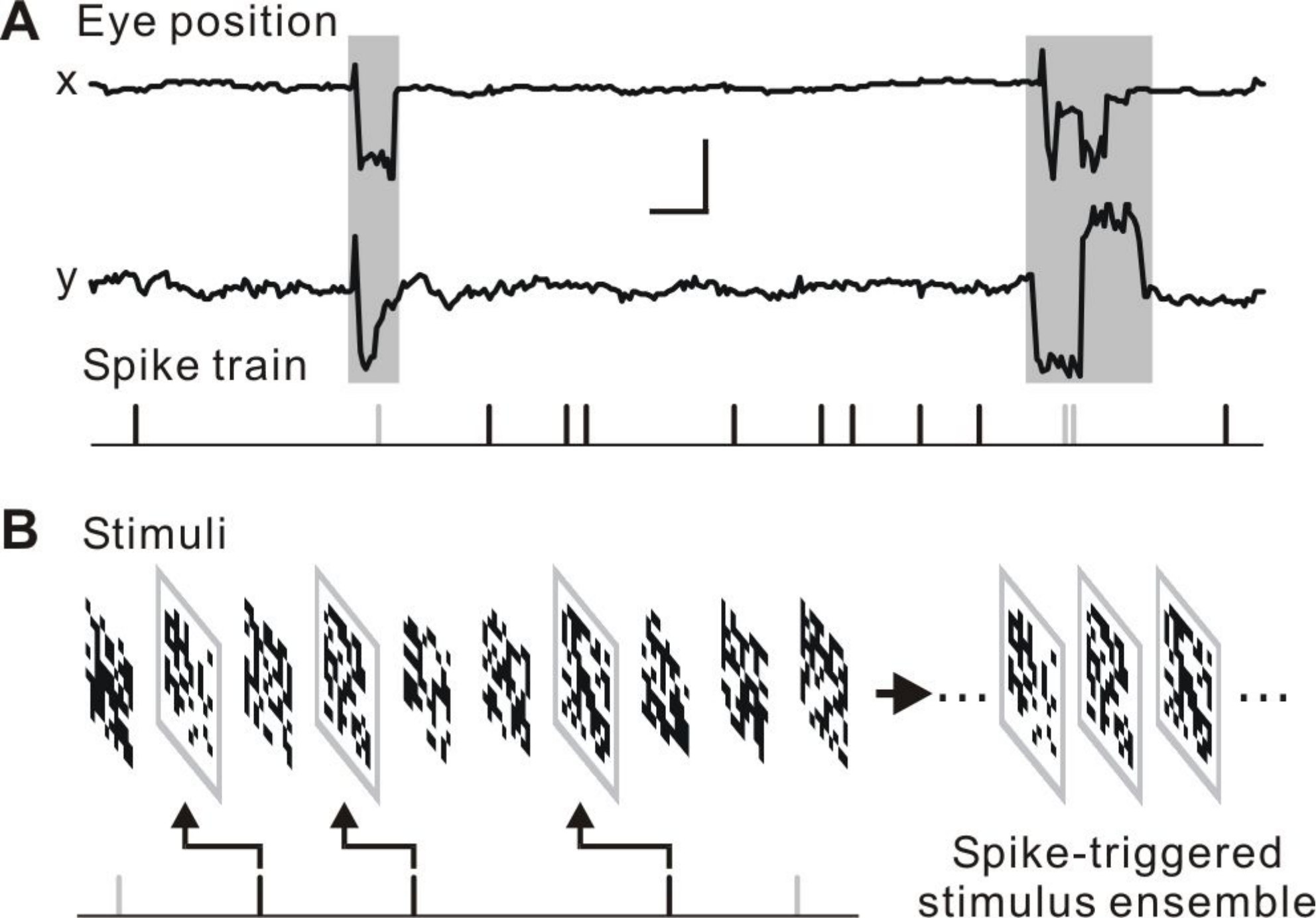
A
Eye position
x
y
Spike train
B
Stimuli
Spike-triggered
stimulus ensemble

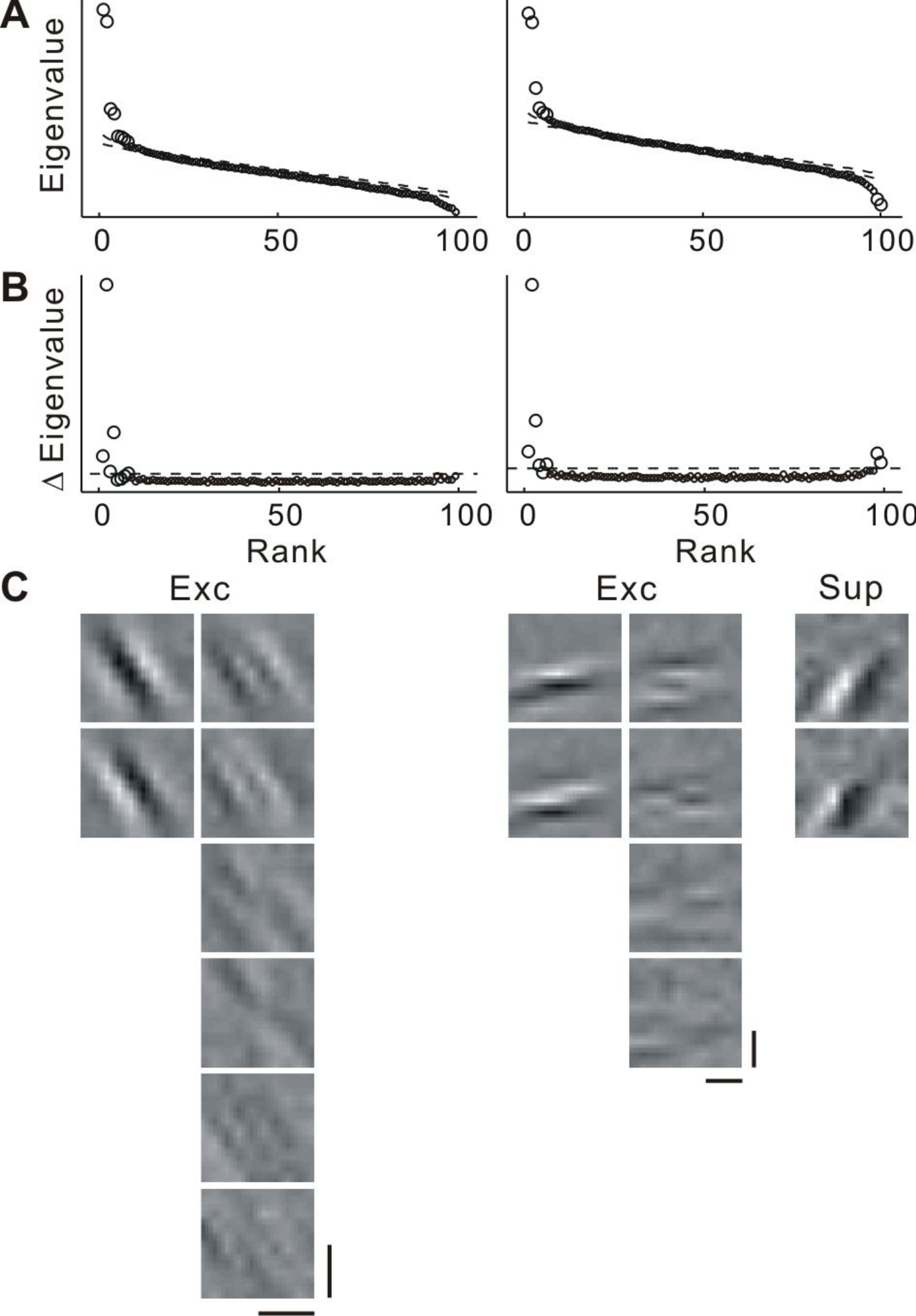
A
Eigenvalue
0
50
100
0
50
100
B
Δ Eigenvalue
0
50
100
Rank
0
50
100
Rank
C
Exc
Exc
Sup

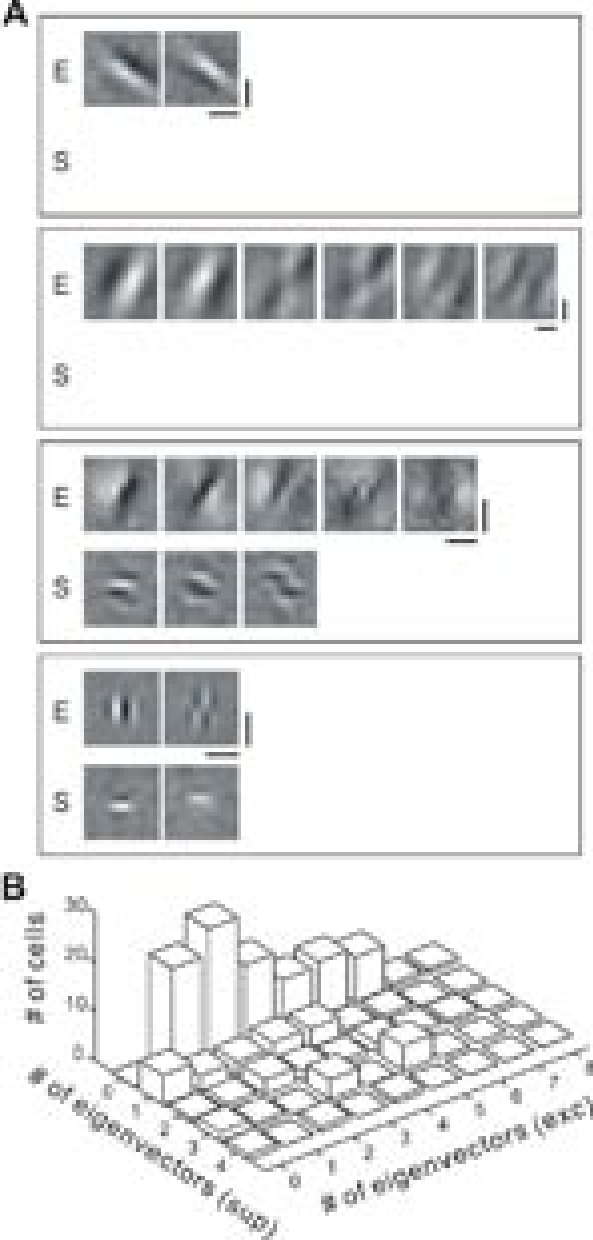
A
E
S
E
S
E
S
E
S
B
# of cells
30
20
10
0
# of eigenvectors (sup)
0 1 2 3 4
# of eigenvectors (exc)
0 1 2 3 4 5 6 7

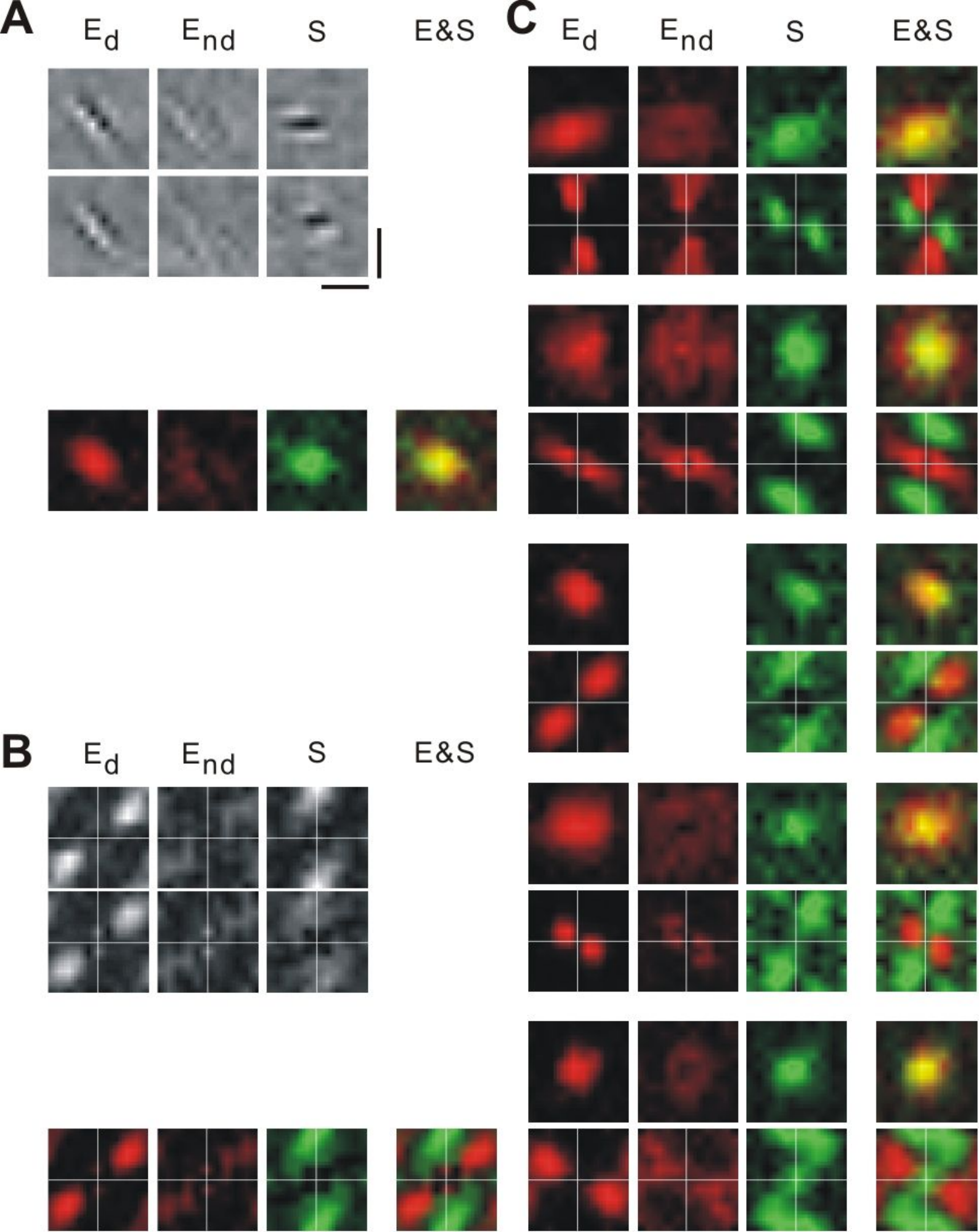
A
E_d
E_{nd}
S
E&S
B
E_d
E_{nd}
S
E&S
C
E_d
E_{nd}
S
E&S

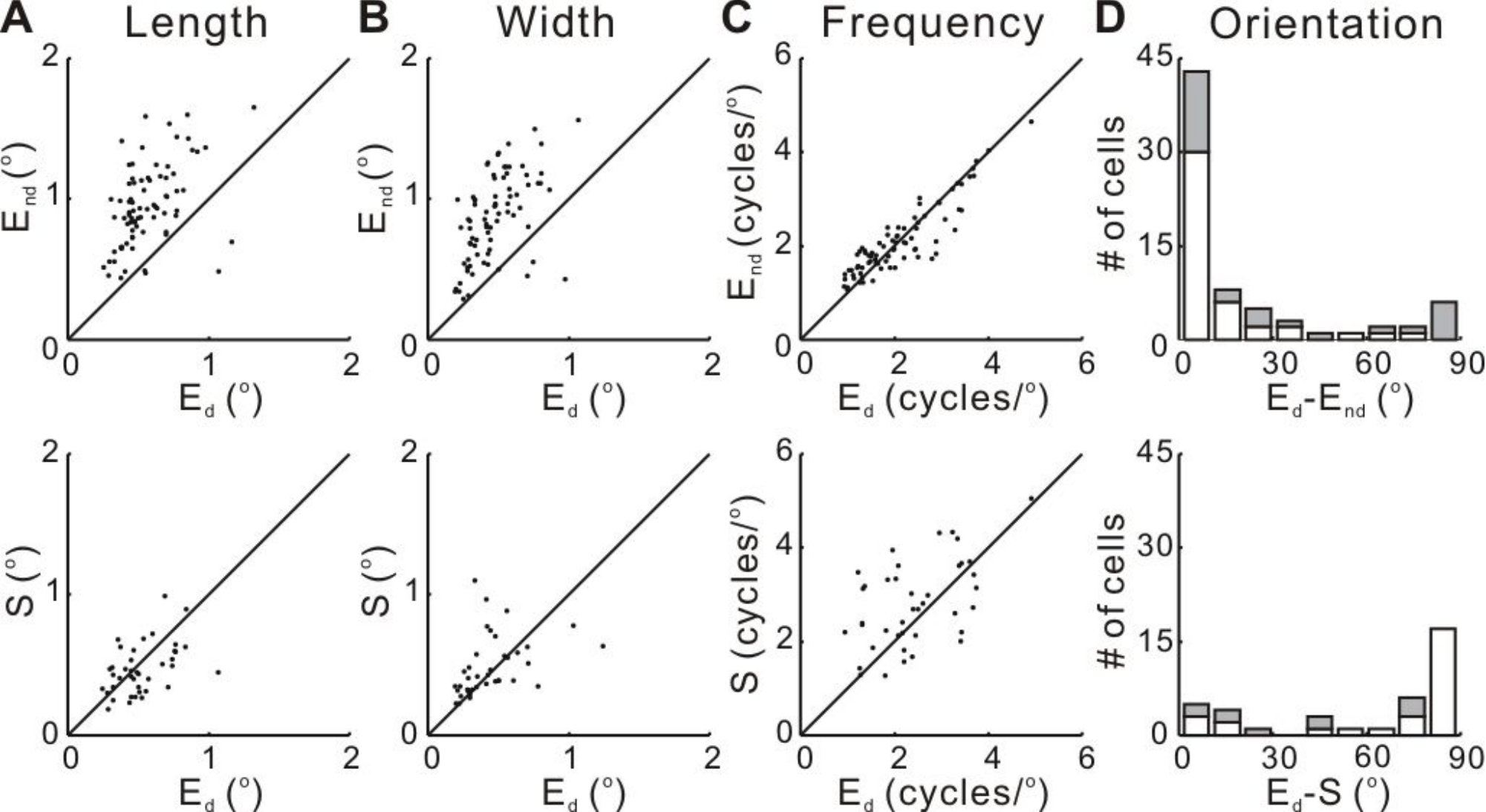
A
Length
B
Width
C
Frequency
D
Orientation
E_{nd} (°)
E_d (°)
E_{nd} (cycles/°)
E_d (cycles/°)
# of cells
E_d-E_{nd} (°)
S (°)
S (cycles/°)
E_d-S (°)
0
1
2
4
6
15
30
45
60
90

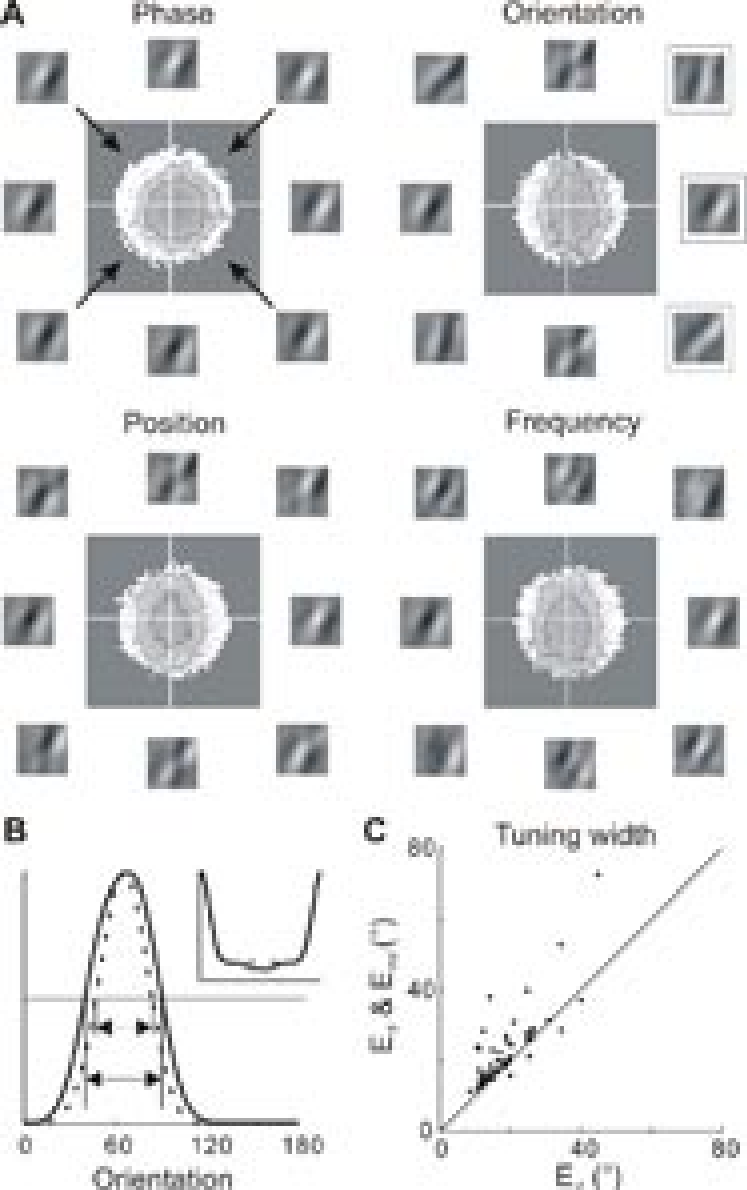
A
Phase
Orientation
Position
Frequency
B
0
60
120
180
Orientation
C
Tuning width
80
40
0
0
40
80
E_1 ± E_2 (°)
E_1 (°)

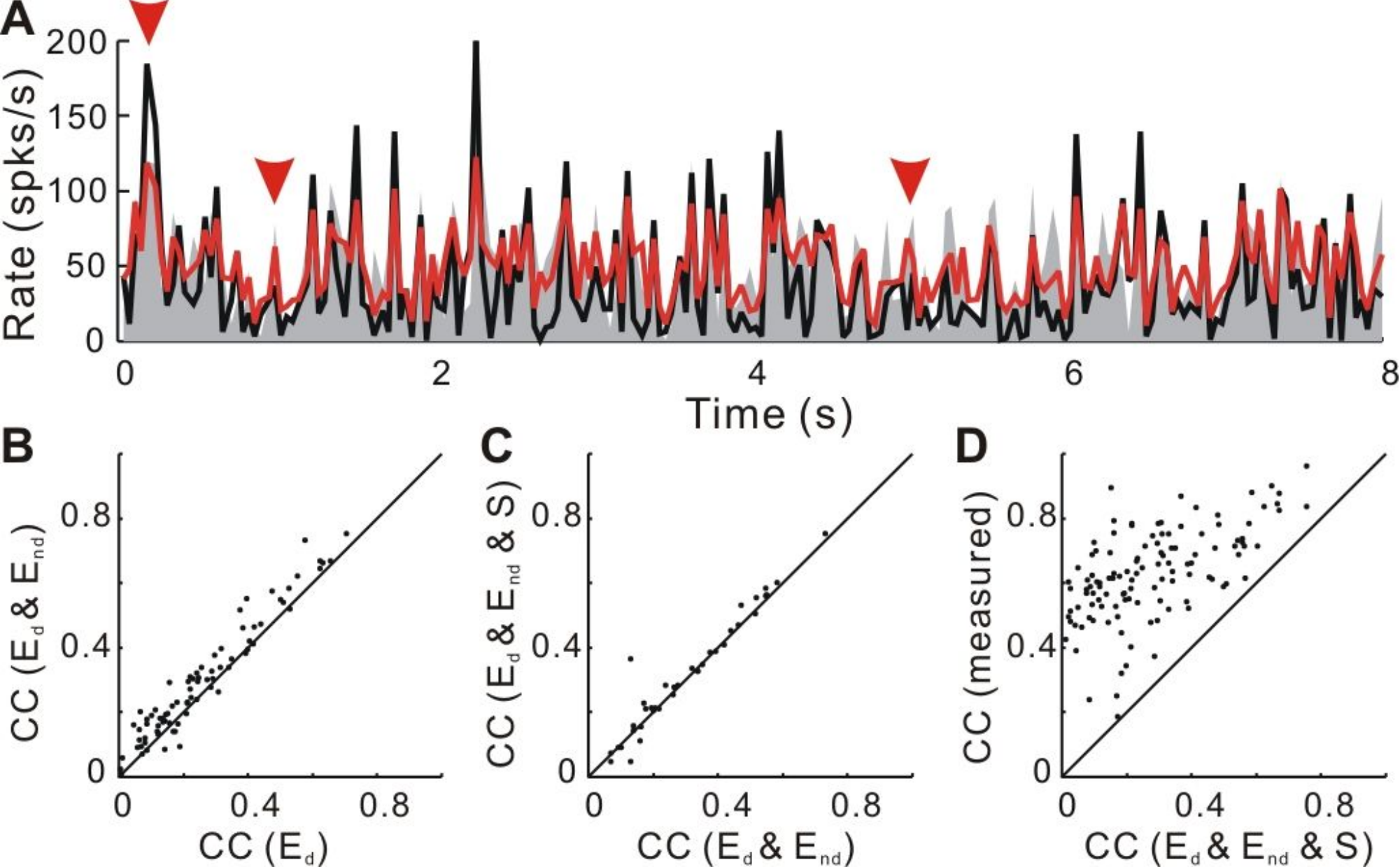
A
Rate (spks/s)
200
150
100
50
0
0
2
4
6
8
Time (s)
B
CC (E_d & E_nd)
0.8
0.4
0
0
0.4
0.8
CC (E_d)
C
CC (E_d & E_nd & S)
0.8
0.4
0
0
0.4
0.8
CC (E_d & E_nd)
D
CC (measured)
0.8
0.4
0
0
0.4
0.8
CC (E_d & E_nd & S)